

# Kalb-Ramond field localization on the Bloch brane

W. T. Cruz\*

*Instituto Federal de Educação, Ciência e Tecnologia do Ceará (IFCE),  
Campus Juazeiro do Norte, 63040-000 Juazeiro do Norte-Ceará-Brazil*

R. V. Maluf<sup>†</sup> and C. A. S. Almeida<sup>‡</sup>

*Universidade Federal do Ceará, Departamento de Física - Campus do Pici,  
C.P. 6030, 60455-760, Fortaleza-Ceará-Brazil*

## Abstract

This work deals with new results on the Kalb-Ramond (KR) field localization in braneworld models. We consider a five-dimensional warped spacetime with an embedded AdS4 thick brane which is generated by two real scalar fields coupled with gravity (the so called Bloch brane). We find a KR field zero mode localized with the inclusion of the dilaton coupling. Analyzing the massive spectrum, we detected a series of resonant modes that arise from the solutions of the Schrödinger-like equation for KR field. The effects of the brane thickness and of the dilaton coupling over the resonance structures are determined. Such analysis is extended to the resonance lifetimes of the massive modes, allowing a better understanding on the localization mechanism of the model.

PACS numbers: 11.10.Kk, 11.27.+d, 04.50.-h, 12.60.-i

---

\*Electronic address: wilami@fisica.ufc.br

<sup>†</sup>Electronic address: r.v.maluf@fisica.ufc.br

<sup>‡</sup>Electronic address: carlos@fisica.ufc.br

## I. INTRODUCTION

Over the past years, braneworld models have been proposed as an alternative solution to solve the hierarchy and the cosmological constant problems [1–3]. Such models consider the gravity free to propagate into the extra dimension, while the matter fields are constrained to propagate only on the brane. However, some problems were encountered to localize the standard model (SM) fields in Randall-Sundrum (RS) scenario, such as spin-1 fields [4]. In this way, to circumvent these problems and to keep the idea of braneworlds, some works have considered a five-dimensional spacetime (bulk) where the observable universe (brane) is taken as a topological defect with solutions that may be interpreted as non-singular versions of the RS scenario [5, 6].

Topological defects like domain walls have been used to represent braneworld models with one extra dimension [5, 7, 8]. Such models can be constructed from scalar fields coupled to gravity, giving rise to thick branes scenarios. Some of these models may be used to mimic new braneworlds containing internal structures [9] with implications on the density of matter-energy along the extra dimensions [10]. The advantages of these models over the RS model is that they are non-singular and dynamically generated. Moreover, the warp factor is a smooth function determined by the scalar potential. In this work we consider a Bloch brane model [11], which is constructed from two real scalar fields coupled with gravity. Such model admits internal structure and the defect thickness is controlled by a real parameter. Recently, the localization of gravity [11], fermions [12, 13] and gauge fields [14] have been considered in this context.

Within this context, we propose to analyze the location of a rank-2 antisymmetric tensor gauge field, known as Kalb-Ramond (KR) field. The field strength tensor for KR field  $H_{MNQ}$  is usually related with a Riemann-Cartan spacetime with torsion [15]. Recent studies at the RS scenario on this background have associated the presence of the torsion for KR field, which can exist together with gravity even outside of the brane [16].

From previous results obtained in thick brane models, we see that the dilaton scalar field is required to be added to the background and to interact directly with gauge fields in order to obtain normalized zero mode solutions [17]. The same coupling was introduced in Refs. [18–20] to study the behavior of vector and tensor gauge fields in branes generated by kinks. In string theory, the dilaton is considered a scalar partner of the spin-2 graviton

and determines the string coupling constant [21]. Furthermore, the dilaton-matter coupling violates the equivalence principle, as shown in Ref. [22]. In Ref. [23] the authors consider the dilaton and moduli supermultiplets as candidates for dark matter, showing evidences of low-energy physics in string theory. Motivated by these results, we propose to apply the same technique to analyze the behavior of the KR field on the Bloch brane. As we will see, the thickness defect will influence the coupling of the massive modes with matter, as well as the intensity of the dilaton coupling with the KR field.

This work is organized as follows. In Sec. II, we present the Bloch brane scenario added to the dilaton coupling. In Sec. III we search for a zero mode localized for the KR field on the previous setup. In Sec. IV, we analyze the massive spectrum and search for resonance structures. Finally, we present our conclusions in Sec. V.

## II. DILATONIC BLOCH BRANE SETUP

In this section we introduce the thick brane scenario that we consider to study the localization of tensor gauge fields. The basic Bloch brane background, as previously studied in references [11–13], is unable to localize the KR field zero mode [19]. Indeed, the tensor gauge field geometry associated with the warp factor leads to a divergent effective action. Thus, an interesting question is the investigation of how the KB field can be localized. In this context, a mechanism largely used to allow the localization of fields in thick brane setups [17–20, 24] consists in adding the dilaton field in the matter sector. So, we will study the features of the KR field in a scenario named *dilatonic Bloch brane*, defined by the action

$$\mathcal{S} = \int d^5x \sqrt{-G} \left[ \frac{1}{4} R - \frac{1}{2} (\partial\phi)^2 - \frac{1}{2} (\partial\chi)^2 - \frac{1}{2} (\partial\pi)^2 - V(\phi, \chi, \pi) \right], \quad (1)$$

where  $G = \det(G_{AB})$  and  $R$  is the Ricci scalar, with Latin indices used for the bulk coordinates. The brane is composed by the two fields  $\phi$  and  $\chi$  which depend only on the extra dimension  $y$ . Following the reference [17], we maintain the fields  $\phi$  and  $\chi$  and include the dilaton scalar field  $\pi(y)$  that will couple directly with the KR field. The differences of the dilaton to the other scalar fields will be clarified when we complete the background description. The geometric framework is an AdS five dimensional spacetime with the following metric

$$ds^2 = e^{2A(y)} \eta_{\mu\nu} dx^\mu dx^\nu + e^{2B(y)} dy^2, \quad (2)$$

where  $A(y)$  and  $B(y)$  are warp factors to be determined by the Einstein equations. The Minkowski metric  $n_{\mu\nu}$  is diagonal with entries  $(-1, 1, 1, 1)$  and Greek indices vary from 1 to 4. The equations of motion coming from the action are

$$\begin{aligned}\phi'^2 + \chi'^2 + \pi'^2 - 2e^{2B}V &= 6A'^2 \\ \phi'^2 + \chi'^2 + \pi'^2 + 2e^{2B}V &= -6A'^2 + 3A'B' - 3A'' \\ \gamma'' + (4A' - B')\gamma' &= e^{2B}\partial_\gamma V, \quad \text{with } \gamma = \phi, \chi, \pi,\end{aligned}\tag{3}$$

where prime stands for derivative with respect to  $y$ .

Therefore, we can obtain first-order differential equations from the Eq. (3) by taking the potential in terms of a superpotential  $W(\phi, \chi)$  [25–27]. To maintain the Bloch brane structure we consider the following potential function [17]

$$V = e^{\pi\sqrt{\frac{2}{3}}} \left[ \frac{1}{8} \left( \frac{\partial W}{\partial \phi} \right)^2 + \frac{1}{8} \left( \frac{\partial W}{\partial \chi} \right)^2 - \frac{5}{16} W^2 \right].\tag{4}$$

We obtain first-order differential equations that solve the equations of motion

$$\begin{aligned}\phi' &= \frac{1}{2} \frac{\partial W}{\partial \phi}, \quad \chi' = \frac{1}{2} \frac{\partial W}{\partial \chi} \\ \pi &= -\sqrt{\frac{3}{8}} A, \\ B &= \frac{A}{4} = -\frac{\pi}{2} \sqrt{\frac{2}{3}}, \\ A' &= -\frac{W}{3}.\end{aligned}\tag{5}$$

The Bloch brane model is obtained by the following superpotential function [28–30]

$$W(\phi, \chi) = 2\phi - \frac{2}{3}\phi^3 - 2r\phi\chi^2,\tag{6}$$

and we obtain the solutions to the scalar fields modeling the brane as

$$\phi(y) = \tanh(2ry),\tag{7}$$

and

$$\chi(y) = \sqrt{\left(\frac{1}{r} - 2\right)} \operatorname{sech}(2ry).\tag{8}$$

The factor  $r$  is a real parameter that controls the brane thickness. We can see that for the limit  $r = \frac{1}{2}$ , the one-field scenario is recovered.

The warp factor obtained is

$$A(y) = \frac{1}{9r} \left[ (1 - 3r) \tanh^2(2ry) - 2 \ln \cosh(2ry) \right]. \quad (9)$$

This brane model supports internal structure which influences the matter energy density along the extra dimension. We can find more details about this feature and graphical analysis of the solutions (7,8, and 9) in the reference [11].

### III. KALB-RAMOND FIELD ZERO MODE

After define the brane scenario, the next step is to analyze the localization of the KR field zero mode and the influence of the dilaton coupling. The dilaton field will couple directly with the KR field in a combination defined by the action [31, 32]:

$$S \sim \int d^5x \sqrt{-G} (e^{-\lambda\pi\sqrt{\frac{8}{3}}} H_{MNL} H^{MNL}), \quad (10)$$

where  $H_{MNL} = \partial_{[M} B_{NL]}$  and  $\lambda$  is a constant that controls the intensity of the dilaton coupling. Therefore, we must analyze the equations of motion for the tensor gauge field in the dilatonic Bloch brane background. This equation takes the form

$$\partial_M (\sqrt{-G} G^{MP} G^{NQ} G^{LR} e^{-\lambda\pi\sqrt{\frac{8}{3}}} H_{PQR}) = 0. \quad (11)$$

With the gauge choice  $B_{\alpha 5} = \partial_\mu B^{\mu\nu} = 0$  and with the separation of variables  $B^{\mu\nu}(x^\alpha, y) = b^{\mu\nu}(x^\alpha)U(y) = b^{\mu\nu}(0)e^{ip_\alpha x^\alpha}U(y)$  where  $p^2 = -m^2$ , it is obtained a differential equation which give us information about the extra dimension, namely

$$\frac{d^2 U(y)}{dy^2} - [\lambda\pi'(y)\sqrt{\frac{8}{3}} + B'(y)] \frac{dU(y)}{dy} = -m^2 e^{2[B(y)-A(y)]} U(y) \quad (12)$$

To solve the equation (12) for zero mode  $m = 0$ , we use the following relation

$$\frac{dU(y)}{dy} = g(y), \quad (13)$$

and obtain a solution for  $g(y)$  as

$$g(y) = k e^{[\lambda\pi(y)\sqrt{\frac{8}{3}} + B(y)]}, \quad k = g(0) e^{-[\lambda\pi(0)\sqrt{\frac{8}{3}} + B(0)]}. \quad (14)$$

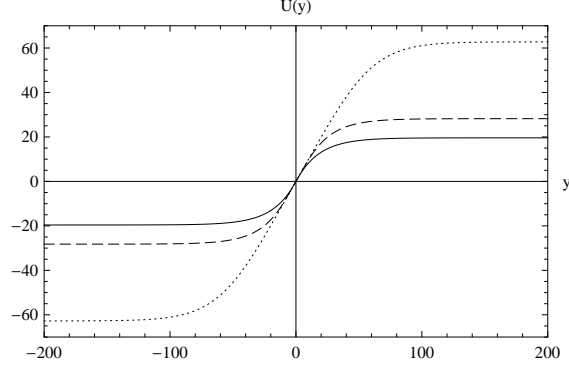


Figure 1: Plots of the solution  $U(y)$  in equation (15) with  $r = 0.01$  (points),  $r = 0.05$  (dashed line) and  $r = 0.25$  (solid line). We have put  $\lambda = 1/8$ .

Using the relations (5) we find a solution for the zero mode of the KR field as a function of the extra dimension given by

$$U(y) = k \int_{y_0}^y e^{(\frac{1}{4}-\lambda)A(y')} dy'. \quad (15)$$

The above solution is finite for  $\lambda < \frac{1}{4}$  where it interpolates between two constant values on both sides of the membrane when  $y \rightarrow \pm\infty$ . The solution (15) is plotted in Figure (1). As we can see, there is a transition region which separates the two interfaces. The thickness of this region as well as the thickness of the defect is controlled by the parameter  $r$ . In this case, when increasing  $r$  the thickness of the transition region is reduced.

Despite we obtain a finite solution, we still cannot guarantee the existence of a zero mode localized. The effective action for the zero mode in five dimensions is

$$S \sim \int d^5x \sqrt{-G} (e^{-\lambda\pi} H_{MNL} H^{MNL}) = \int dy (U(y))^2 e^{A(y)(\lambda-\frac{7}{4})} \int d^4x (h_{\mu\nu\alpha} h^{\mu\nu\alpha}). \quad (16)$$

We observe that for  $\lambda < \frac{1}{4}$ , the condition to have a finite solution for  $U(y)$ , we obtain a divergent effective action. However, a particular solution of the equation of motion (12) is simply  $U(y) \equiv \text{cte}$ . Given the solution  $U(y)$  constant it is possible to show that the integral in the  $y$  variable on the effective action is finite if  $\lambda > \frac{7}{4}$ . As a consequence, for a specific value of the coupling constant  $\lambda$  it is possible to obtain a localized zero mode of the KR field.

#### IV. MASSIVE SPECTRUM AND RESONANCES

In order to analyze the massive modes in this background, we make use of the Eq. (12) and the relations obtained in Eq. (5). Thus, we get

$$\frac{d^2 U(y)}{dy^2} - \alpha A'(y) \frac{dU(y)}{dy} = -m^2 e^{-\frac{3}{2}A(y)} U(y), \quad (17)$$

where  $\alpha = \frac{1}{4} - \lambda$ . Performing the following transformations

$$dz = dy e^{-\frac{3}{4}A}, \quad U = e^{(\frac{\alpha}{2} + \frac{3}{8})A} \overline{U}, \quad (18)$$

we can write the Eq. (17) as a Schrödinger-like equation in the form

$$\left\{ -\frac{d^2}{dz^2} + \overline{V}(z) \right\} \overline{U} = m^2 \overline{U}, \quad (19)$$

with the potential  $\overline{V}(z)$  given by

$$\overline{V}(z) = [\beta^2 (\dot{A})^2 - \beta \ddot{A}], \quad \beta = \frac{\alpha}{2} + \frac{3}{8}, \quad (20)$$

where the dot stands for derivative with respect to  $z$ .

The Schrödinger-like equation (19) can be rewritten in the formalism of supersymmetric quantum mechanics as follows:

$$Q^\dagger Q \overline{U}(z) = \left\{ \frac{d}{dz} - \beta \dot{A} \right\} \left\{ \frac{d}{dz} + \beta \dot{A} \right\} \overline{U}(z) = -m^2 \overline{U}(z). \quad (21)$$

Now looking at the form of the Eq. (21), we can exclude the possibility of the normalized negative energy modes exist [33].

The mass spectrum is determined by the characteristics of the potential at infinity. If  $\overline{V} \rightarrow 0$  when  $z \rightarrow \infty$ , then we have a continuous gapless spectrum of Kaluza-Klein states. Due to the transformations in Eq. (18), we cannot achieve the analytical structure of the potential  $\overline{V}(z)$  and hence, the wave functions for the massive modes that are solutions of the Eq. (21) does not have an analytical representation. However, we will be able to analyze  $\overline{V}(z)$  numerically.

In Fig. 2 we have shown  $\overline{V}(z)$  for some values of constants  $\lambda$  and  $r$ . Observing the asymptotic behaviour of the potential, we conclude that  $\lim_{z \rightarrow \infty} \overline{V}(z) = 0$  and the continuum spectrum is gapless. The most relevant information that we can extract from these graphs refers to the maximum points of the potential. The solutions of massive modes on

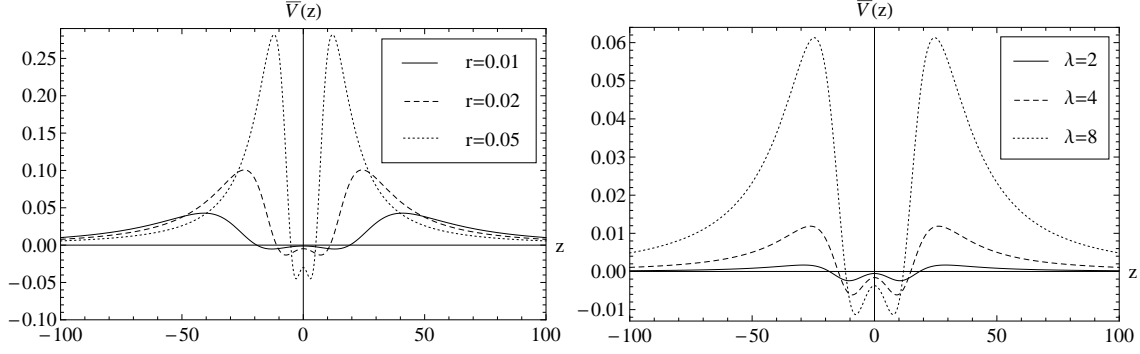


Figure 2: Plots of  $\bar{V}(z)$  for  $\lambda = 10$  (left) and  $r = 0.01$  (right).

the brane depends on the maximum value of the potential, but for  $m^2 \gg \bar{V}_{\max}$  this dependence becomes negligible. However, when we have  $m^2 < \bar{V}_{\max}$  the potential structure will influence the solution of the massive modes near  $z = 0$ .

Looking still to Fig. 2, we see that raising the value of the dilaton coupling constant implies an increasing in the maximum value of the potential. The same feature is observed when increasing the value of  $r$ , i.e., when one grows up the thickness of the brane.

For a given potential we must know the behaviour of the solutions  $\bar{U}(z)$  in relation to their masses. With this purpose, we plot in Fig. (3) the solutions of  $\bar{U}(z)$  for  $m = 1$  (left) and  $m = 20$  (right). In both cases, we use the same potential, while keeping constant  $\lambda$  and  $r$ . The light modes ( $m^2 < \bar{V}_{\max}$ ) are suppressed in the region between the maxima of the potential and in the region distant from the brane, where they can be approximated by plane wave solutions. However, the modes in which  $m^2 \gg \bar{V}_{\max}$  possess plane wave solution across all extra dimension. It is worth noting that either the dilaton coupling as well as the brane thickness affect the solutions of the massive modes in the extra dimension. Thus, these two constants modify the coupling of the tensor gauge field with the matter on the brane.

A very interesting feature is that although the massive modes with  $m^2 < \bar{V}_{\max}$  are suppressed at  $z = 0$ , there is a possibility that for some specific values of masses, the plane wave solutions of the Schrödinger equations can resonate with the potential, yielding resonance modes [5, 34, 35]. Such structures exhibit very large solutions within the brane, when comparing its value when  $z \rightarrow \infty$ . In order to search for resonances, we must know the solutions of  $\bar{U}(z)$  at  $z = 0$  with respect to the mass. In this way, we take the probability density of the wave function at the center of the brane  $P(m) = |\zeta \bar{U}(0)|^2$ , where  $\zeta$  is a



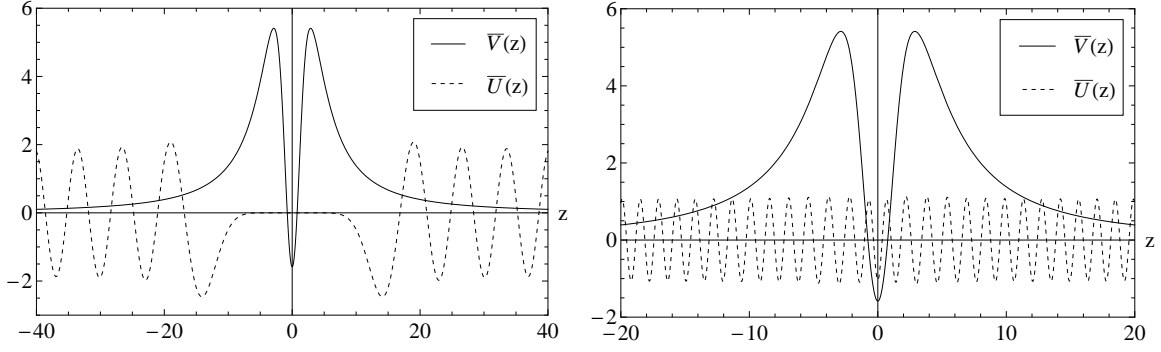


Figure 3: Plots of  $\bar{V}(z)$  and  $\bar{U}(z)$  for  $m = 1$  (left) and  $m = 20$  (right). We put  $\lambda = 20$  and  $r = 0.25$  in two graphics.

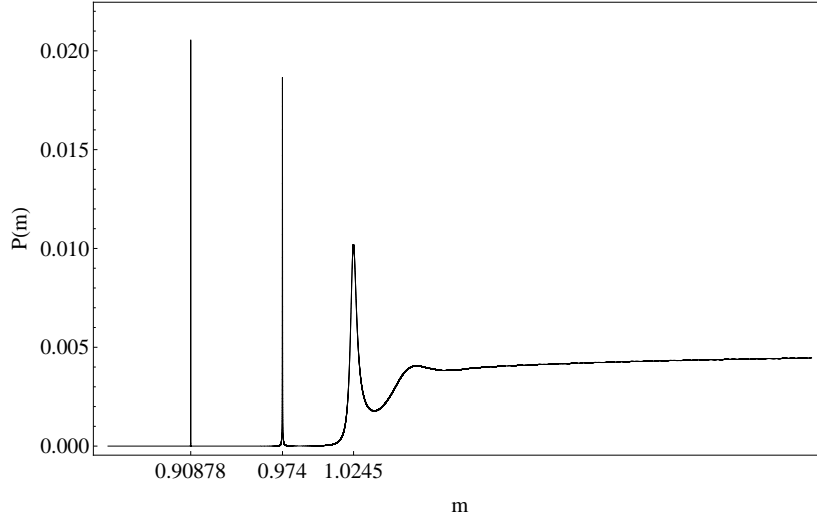


Figure 4: Plots of  $P(m)$  with  $\lambda = 46$  and  $r = 0.01$ . We note three resonance peaks with masses  $m = 0.90878$ ,  $m = 0.9740$  and  $m = 1.0245$  with lifetimes  $\tau = 1.00 \times 10^5$ ,  $\tau = 5.55 \times 10^3$  and  $\tau = 1.76 \times 10^2$  respectively.

normalization constant taken at the box  $-200 < z < 200$ .

In Fig. (4) we present  $P(m)$  for  $\lambda = 46$  and  $r = 0.01$ . It is observed the existence of three resonances in  $m = 0.90878$ ,  $m = 0.9740$  and  $m = 1.0245$ . The difference among them, besides the masses, is determined by their lifetimes. We can estimate the lifetime  $\tau$  of a resonance by  $(\Delta m)^{-1}$ , where  $\Delta m$  is the width at half maximum in mass of the peaks in  $P(m)$  [13, 36–38, 42].

Regarding solutions of the Schrödinger equation, resonances with higher lifetimes charac-

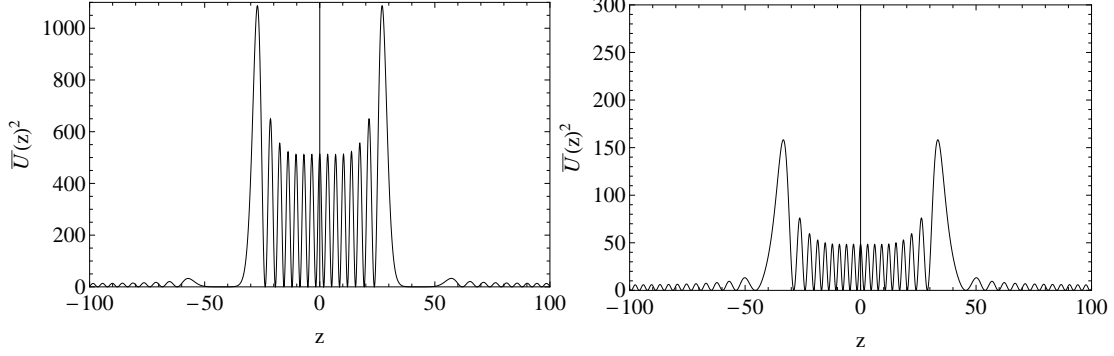


Figure 5: Plots of  $\overline{U}(z)^2$  with masses  $m = 0.90878$  (left) and  $m = 1.0245$  (right) where we have put  $\lambda = 46$  and  $r = 0.01$ . Note that these two masses correspond to resonances as shown in Fig. (4).

terize solutions of  $\overline{U}(z)$  with large amplitudes on the brane location. To better understand this feature, we present in Fig. (5) the solutions for two resonant modes as seen in Fig. (4). The selected masses were  $m = 0.90878$  and  $m = 1.0245$  with lifetime  $\tau = 1.00 \times 10^5$  and  $\tau = 1.76 \times 10^2$ , respectively. The solution for the resonant mode with the highest lifetime (left) has a wider amplitude at  $z = 0$ , when compared with another one (right). This shows us that these modes are highly coupled with matter on the brane, as compared to the non-resonant modes. The calculation of  $\tau$  is also useful to show which peaks in  $P(m)$  can be considered resonances. For example, in situations where  $\Delta m$  greater than the peak position  $m$ , the lifetimes are so small that they do not produce any measurable effects. Thus, these modes cannot be considered resonances.

Another question is whether the resonance structures may be affected by the intensity of the dilaton coupling, as well as the thickness of the defect. This issue can be better understood by knowing how the masses of the resonant modes are modified according to the constants  $\lambda$  and  $r$ . Excluding cases with very small lifetimes, we shown in Fig. (6) a series of mass values of peaks obtained in terms of  $P(m)$  as a function of  $\lambda$  and  $r$ . The connected points correspond to the same resonance structure. As we can see, increasing the values of  $\lambda$  or  $r$  the masses of the peaks in the probability density function increases too. Therefore, raising  $\lambda$  or  $r$  implies an increase of the mass in each resonance spectrum. In general, the mass range where the resonances appear correspond to larger values of  $m$ , as  $r$  or  $\lambda$  increase. This is connected to the characteristics of the potential  $\overline{V}(z)$  to the KR field. The maximum potential is raised when we increase  $\lambda$  or  $r$  so that the light modes are suppressed in the

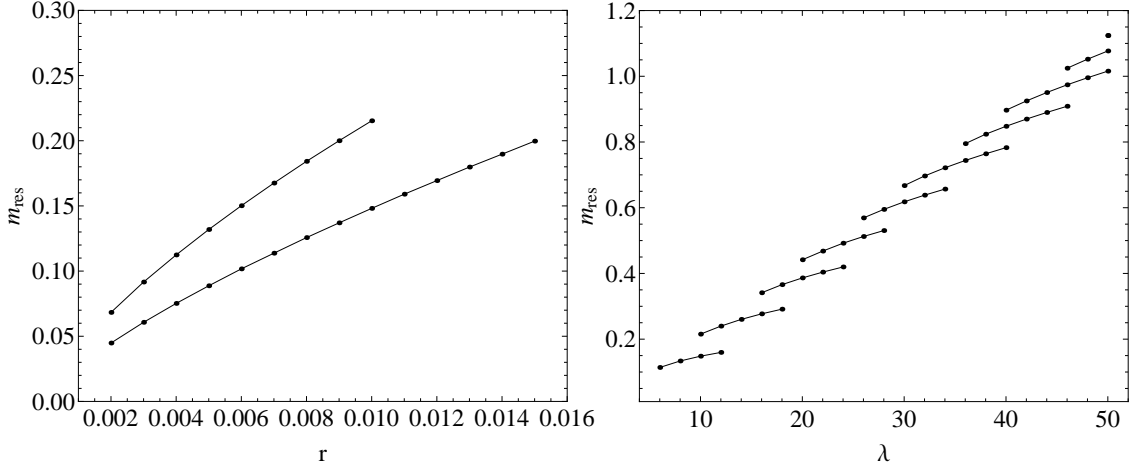


Figure 6: Plots of the resonance masses in function of  $r$  (left) and  $\lambda$  (right). We have put  $\lambda = 10$  (left) and  $r = 0.01$  (right).

region near  $z = 0$  and resonant modes appear for bigger masses.

Let us now consider what happens when the defect thickness is changed on the resonant modes. First we note that for  $r = 0.002$  (See Fig. 6, left) there are two resonances in the spectrum. However, when  $r = 0.015$  there is only one resonance. The one with greater mass, represented by the upper line in Fig. 6 (left), it vanishes near  $r = 0.01$ . On the other hand, increasing the value of  $\lambda$  as seen in Fig.6 (right), we observe a slight uptick in the number of resonances. This behaviour can be understood through the relation on lifetimes of resonance with respect to the parameters  $r$  and  $\lambda$ . In Table I, we display some values of  $r$  and  $\lambda$ , and the corresponding lifetimes. As can be seen, an increase in  $r$  corresponds to a reduction on the resonance lifetimes, and the opposite happens for  $\lambda$ . This feature explains why we have more resonances when increasing  $\lambda$  or reducing  $r$  [13].

## V. CONCLUSIONS

Concerning the localization in thick brane models, many studies show that the KR field cannot have zero mode localized on the usual Bloch brane setup [11–13]. Actually, in these papers it was found that the solutions of the equation of motion for the KR field yield a divergent effective action, breaking the localization mechanism.

Aiming to overcome this result, we employ a well-known method within the context of the localization for gauge and tensor gauge fields on the branes [17–19, 24]. It consists of

$\lambda = 10$				$r = 0.01$			
r	m	$\Delta m$	$\tau$	$\lambda$	m	$\Delta m$	$\tau$
0.011	0.1590	0.00018	5555.55	30	0.6673	0.0135	74.074
0.012	0.1694	0.00021	4761.90	32	0.6966	0.0035	285.714
0.013	0.1798	0.00025	4000	34	0.7215	0.00084	1190.47
0.014	0.1897	0.00028	3571.4	36	0.7950	0.00017	5882.35
0.015	0.1997	0.00033	3030.3	38	0.8237	0.000027	37037.4

Table I: The mass, width and lifetimes of resonances in function of  $\lambda$  and  $r$ .

adding an extra field to the model, the dilaton, which coupled to the KR field, enabled us to locate a zero mode on the Block brane.

Moreover, we rewrite the equation of motion for the KR field as a Schrödinger-like equation, and from the analysis of the massive modes we conclude that the spectrum is free of negative energy states. In particular, light mode states are suppressed in the region among the maxima of the potential. Nevertheless, there are some solutions for certain masses values that have large amplitudes at  $z = 0$ , and which can be characterized as being resonances.

To detect the resonant modes we use a technique widely applied in the context of thick branes [13, 14, 19, 20, 37–44] based on the calculation of the probability density of the wave function. We have normalized the wave functions in a box so that its borders are far from the turning points. As noted in Ref. [13], the choice of the size of the box has no physical significance, since if it is chosen sufficiently large, it does not interfere with the position of the resonant modes.

To complete the study of the massive spectrum we calculate the value of the lifetimes of resonant modes in addition to analyzing the conditions under which they can be changed. As noted, the lifetime value helps us to know the shape of the resonant modes solution as well as its coupling with the membrane. Narrow peaks on the probability density function correspond to higher lifetimes, so that they characterize large amplitudes at  $z = 0$  for the solutions of the Schrödinger equation.

When we increase the thickness of the defect the lifetime of resonances is reduced. This characteristic was also observed for the resonances found in the study of fermions localization in Bloch branes [13]. Opposite effect occurs when raise the intensity of the coupling of the

dilaton with the KR field. In this case both the quantity and the lifetime of the resonances is increased. The position of the resonant modes in the mass spectrum is influenced by the value of the coupling constant  $\lambda$ , which when is reduced causes a decrease in the value of the mass of the resonant modes. The same aspect is observed when we change the value of the constant  $r$  that controls the thickness of the membrane.

### Acknowledgments

The authors thank the Fundação Cearense de apoio ao Desenvolvimento Científico e Tecnológico (FUNCAP), the Coordenação de Aperfeiçoamento de Pessoal de Nível Superior (CAPES), and the Conselho Nacional de Desenvolvimento Científico e Tecnológico (CNPq) for financial support.

- 
- [1] L. Randall and R. Sundrum, Phys. Rev. Lett. **83**, 3370 (1999); **83**, 4690 (1999).
  - [2] N. Arkani-Hamed, S. Dimopoulos and G. Dvali, Phys. Lett. B **429**, 263 (1998).
  - [3] I. Antoniadis, N. Arkani-Hamed, S. Dimopoulos and G. Dvali, Phys. Lett. B **436**, 257 (1998).
  - [4] H. Davoudiasl, J.L. Hewett and T.G. Rizzo, Phys. Rev. Lett. **84**, 2080 (2000).
  - [5] M. Gremm, Phys. Lett. B **478**, 434 (2000).
  - [6] O. Dewolfe, D.Z. Freedman, S.S. Gubser and A. Karch, Phys. Rev. D **62**, 046008 (2000).
  - [7] V.A. Rubakov and M.E. Shaposhnikov, Phys. Lett. B **125**, 136 (1983).
  - [8] M. Visser, Phys. Lett. B **159**, 22 (1985).
  - [9] D. Bazeia, J. Menezes, and R. Menezes, Phys. Rev. Lett. **91**, 241601 (2003).
  - [10] D. Bazeia, C. Furtado and A.R. Gomes, J. Cosmol. Astropart. Phys. 0402 (2004) 002.
  - [11] D. Bazeia and A. R. Gomes, J. High Energy Phys. 0405 (2004) 012.
  - [12] L.B. Castro, Phys. Rev. D **83**, 045002 (2011).
  - [13] C. A. S. Almeida, M. M. Ferreira, Jr., A. R. Gomes and R. Casana, Phys. Rev. D **79** 125022 (2009).
  - [14] W. T. Cruz, Aristeu R. P. Lima and C. A. S. Almeida, Phys. Rev. D **87**, 045018 (2013).
  - [15] M. Vasilic and M. Vojinovic, Phys. Rev. D **78**, 104002 (2008).
  - [16] B. Mukhopadhyaya, S. Sen and S. SenGupta, Phys. Rev. Lett. **89**, 121101 (2002) , Erratum-

- ibid. **89**, 259902 (2002).
- [17] A. Kehagias and K. Tamvakis, Phys. Lett. B **504**, 38 (2001).
  - [18] M. O. Tahim, W. T. Cruz and C. A. S. Almeida, Phys. Rev. D **79**, 085022 (2009).
  - [19] W.T. Cruz, M.O. Tahim and C.A.S. Almeida, Europhys. Lett. **88**, 41001 (2009).
  - [20] W.T. Cruz, M.O. Tahim and C.A.S. Almeida, Phys. Lett. B **686**, 259 (2010).
  - [21] T. Damour, Federico Piazza and G. Veneziano, Phys. Rev. Lett. **89**, 081601 (2002).
  - [22] T.R. Taylor and G. Veneziano, Phys. Lett. B **213**, 450 (1988).
  - [23] B. de Carlos, J.A. Casas and F. Quevedo, Phys. Lett. B **318**, 447 (1993).
  - [24] H.R. Christiansen, M.S. Cunha and M.O. Tahim, Phys. Rev. D **82**, 085023 (2010).
  - [25] D. Bazeia, M.J. dos Santos and R.F. Ribeiro, Phys. Lett. A **208**, 84 (1995).
  - [26] D. Bazeia, H. Boschi-Filho, and F.A. Brito, J. High Energy Phys. 9904 (1999) 028.
  - [27] D. Bazeia and F.A. Brito, Phys. Rev. Lett. **84**, 1094 (2000).
  - [28] D. Bazeia, J.R. Nascimento, R.F. Ribeiro and D. Toledo, J. Phys. A **30**, 8157 (1997).
  - [29] M.A. Shifman and M.B. Voloshin, Phys. Rev. D **57**, 2590 (1998).
  - [30] A. Alonso Izquierdo, M.A. Gonzalez Lion and J. Mateos Guilarte, Phys. Rev. D **65**, 085012 (2002).
  - [31] K. Sfetsos and A. A. Tseytlin, Phys. Rev. D **49**, 2933 (1994).
  - [32] B. Kleihaus, J. Kunz and K. Myklevoll, Phys. Lett. B **605**, 151 (2005).
  - [33] D. Bazeia and M.M. Santos, Phys. Lett. A **217**, 28 (1996).
  - [34] C. Csaki, J. Erlich, T. J. Hollowood and Y. Shirman, Nucl. Phys. B **581**, 309 (2000).
  - [35] C. Csaki, J. Erlich, T. J. Hollowood and Y. Shirman, Phys. Rev. Lett. **84**, 5932 (2000).
  - [36] R. Gregory, V. A. Rubakov and S. M. Sibiryakov, Phys. Rev. Lett. **84**, 5928 (2000).
  - [37] Yu-Xiao Liu, Hai-Tao Li, Zhen-Hua Zhao, Jing-Xin Li and Ji-Rong Ren, J. High Energy Phys. 10 (2009) 091.
  - [38] Yu-Xiao Liu, Chun-E Fu, Heng Guo and Hai-Tao Li, Phys. Rev. D **85**, 084023 (2012).
  - [39] W. T. Cruz, A. R. Gomes, C. A. S. Almeida, Eur. Phys. J. C **71**, 1790 (2011).
  - [40] W.T. Cruz, A.R. Gomes and C.A.S. Almeida, Europhys. Lett. **96**, 31001 (2011).
  - [41] W.T. Cruz and C.A.S. Almeida, Eur. Phys. J. C **71**, 1709 (2011).
  - [42] Yu-Xiao Liu, Jie Yang, Zhen-Hua Zhao, Chun-E Fu and Yi-Shi Duan, Phys. Rev. D **80**, 065019 (2009).
  - [43] Yu-Xiao Liu, Chun-E Fu, Li Zhao, Yi-Shi Duan, Phys. Rev. D **80**, 065020 (2009).

[44] Yun-Zhi Du, Li Zhao, Yi Zhong, Chun-E Fu and Heng Guo, arXiv:hep-th/13013204.